THE JOURNAL OF PHYSICAL CHEMISTRY C

Article

pubs.acs.org/JPCC

Multiple Energy Transfer Dynamics in Blended Conjugated Polymer Nanoparticles

Xiaoli Wang, Louis C. Groff, and Jason D. McNeill*

Department of Chemistry, Clemson University, Clemson, South Carolina 29634, United States

Supporting Information

ABSTRACT: Energy transfer dynamics in blended conjugated polymer nanoparticles (CPNs) were investigated in order to further our understanding of photoswitching and anomalous saturation behavior we previously observed, and as a way to probe the complex energy transport processes occurring in similar systems of interest such as nanostructured bulk heterojunction photovoltaic devices. We prepared blended poly[(9,9-dioctylfluorenyl-2,7-diyl)-*co*-(1,4-benzo-{2,1′,3}-thiadiazole)] (PFBT)/poly[2-methoxy-5-(2-ethylhexyloxy)-1,4-phenylenevinylene] (MEH-PPV) nanoparticles with varying blending ratios. Efficient energy transfer from PFBT to MEH-PPV was observed, yielding bright, red-shifted emission. The donor exhibited complex decay kinetics consistent with energy transfer in complex, nanoscale, multichromophoric systems. The fluorescence decay kinetics and steady-state quenching efficiencies are compared to a multiple energy transfer model and prior results for dye-doped nanoparticles. The analysis indicates that the high energy transfer efficiency is largely due to multistep energy transfer (i.e., exciton diffusion), while the lifetime heterogeneity appears to be strongly influenced by acceptor polymer polydispersity as well as nanoscale inhomogeneity. The emerging picture could inform efforts to optimize CPNs for advanced imaging applications, and to optimize energy transport in bulk heterojunction photovoltaic devices.

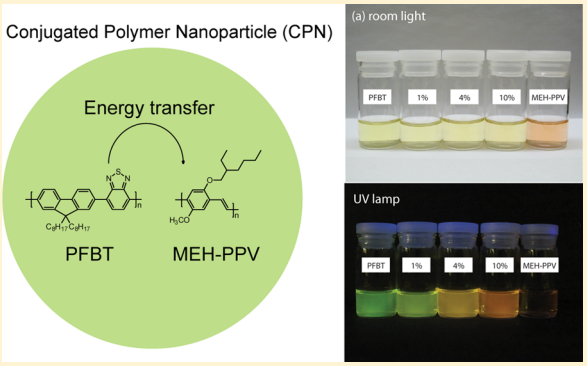

INTRODUCTION

Conjugated polymers have been widely applied for technology applications, such as chemical sensors,[1,2] solar cells,[3] and light emitting devices or displays,[4,5] due to their promising performance, low cost, processability, and tunable optical and electronic properties. Typically, films and powders of conjugated polymers have a disordered structure, described as either glassy or semicrystalline.[6,7] The film preparation conditions to a large extent determine the conformational structure, which in turn dictates the interchromophore interactions and thus the optical and electronic properties of the device.[8,9] The structure and exciton dynamics of blended conjugated polymers are of particular interest due to the performance advantage of devices based on the bulk heterojunction structure formed by polymer blends.[10−14]

The primary neutral electronic excited state in conjugated polymers is typically described as the Frenkel-type molecular exciton, consisting of two or more chromophores quantum-mechanically coupled via transition dipoles.[15,16] The nature of exciton motion in the system varies with the chemical structure, conformation, and processing conditions (as well as other factors such as temperature). In some cases, the conjugated polymer system can be described as a nanoscale collection of weakly coupled chromophores with a moderate or high degree of energetic disorder undergoing Förster transfer between roughly equivalent chromophores,[17,18] sometimes resulting in dispersive transport.[18] In other cases, stronger coupling occurs, resulting in coherent, long-range excitonic interactions and ultrafast transport.[19] There have been extensive investigations of exciton dynamics in conjugated polymer systems, including thin films,[20−22] solutions,[23,24] in a matrix,[25,26] and nanoparticles.[27] Since the structure of polymer blends (bulk heterojunctions) used in photovoltaic devices is often complex, it is desirable to gain a more complete understanding of the electronic and photophysical processes in blended conjugated polymers in order to optimize the device characteristics, as well as how such processes can be modulated through their dependence on structure and processing conditions. It has been proposed to study photophysical processes in blended conjugated polymers in the nanoparticle phase, as an alternative to thin films,[28,29] since more control of various aspects of structure and interactions can be obtained by controlling particle size, and since single nanoparticle experiments can provide a unique window into nanoscale heterogeneity effects and processes such as polaron motion.[30] Furthermore, conjugated polymer nanoparticles (CPNs) have attracted much attention in a variety of applications, such as particle tracking,[31] sensing,[32−34] and cellular imaging,[35,36] because of their small particle size, high fluorescent brightness, and excellent photostability.[37]

Received: August 11, 2014
Revised: October 7, 2014
Published: October 9, 2014

   dx.doi.org/10.1021/jp508147r | J. Phys. Chem. C 2014, 118, 25731−25739

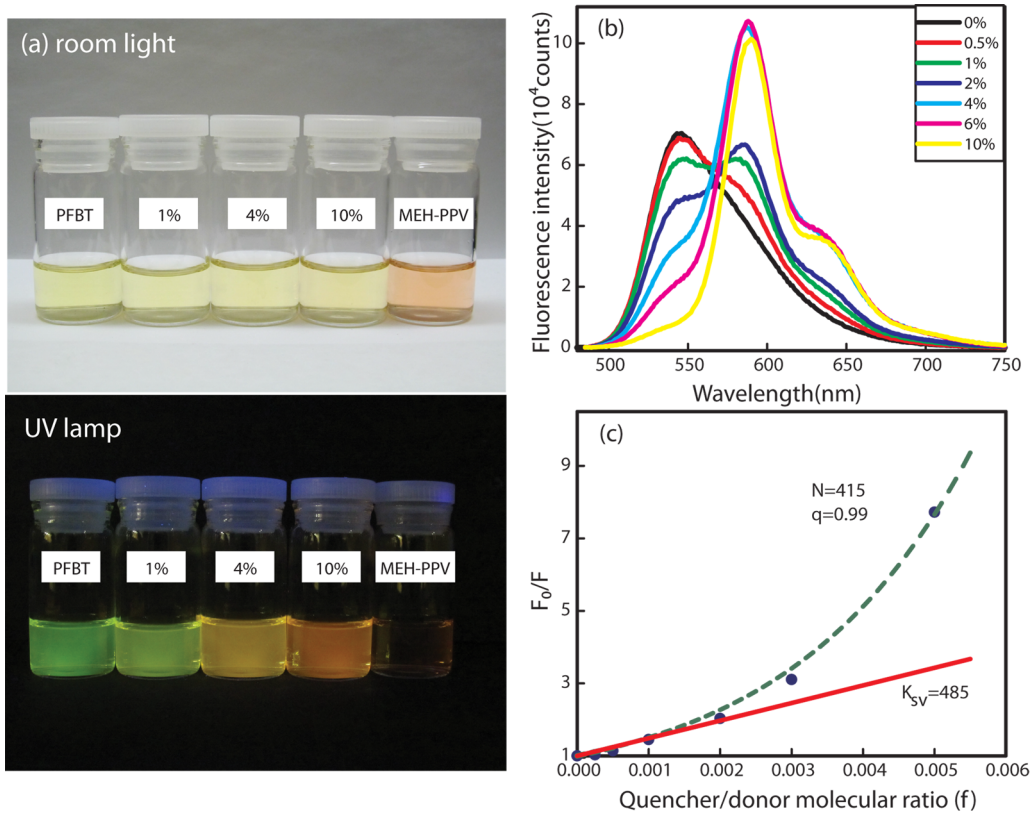

Figure 1. (a) Photographs of aqueous CPNs under room light (top) and UV-lamp (bottom, 365 nm). (b) Concentration-dependent fluorescence spectra of blended polymer nanoparticles under λ_{ex} = 473 nm. (c) Fluorescence quenching of PFBT donor versus quencher/donor molecular ratio. Blue dots are the experimental data, while the red solid line is the fit to the Stern−Volmer equation, and the green dashed line is the fit to the nanoparticle Poisson model.

Previously,[38] we found that blended poly[(9,9-dioctylfluorenyl-2,7-diyl)-*co*-(1,4-benzo-{2,1′,3}-thiadiazole)] (PFBT)/poly[2-methoxy-5-(2-ethylhexyloxy)-1,4-phenylenevinylene] (MEH-PPV) (PFBT/MEH-PPV) CPNs exhibit unusual optical properties. In addition to the expected highly red-shifted emission due to energy transfer, we found anomalous saturation behavior characterized by an extraordinarily low excitation saturation intensity and high saturated brightness, a rare combination of properties that is optimal for saturation-based imaging methods.[39] Additionally, bulk and single nanoparticle spectroscopic experiments indicate that the blended CPNs exhibit photoswitching, which could be useful for localization-based microscopy.[40] Here, we investigate the energy transfer dynamics of blended CPNs through time-resolved and steady-state fluorescence spectroscopies. We observe high energy transfer efficiency, consistent with multistep energy transfer (i.e., exciton diffusion). Picosecond time-resolved fluorescence spectroscopy is used to investigate both the donor and the acceptor, revealing complex decay kinetics of the donor, consistent with multiple energy transfer and a broad range of energy transfer rates. The experimental results are analyzed by comparing to a multiple energy transfer model in order to examine the physical picture of processes occurring in blended CPNs and in an attempt to obtain a clearer picture of the impact and relative importance of multiple energy transfer (energy transfer between donor chromophores) occurring within the donor (host) polymer, energy transfer between donor and acceptor, acceptor conformational effects (e.g., degree of phase separation), acceptor polydispersity, and particle size. Our analysis indicates that multiple energy transfer between donor chromophores greatly increases the effective quenching volume of the acceptor. Additionally, the high energy transfer efficiencies are consistent with a more or less open conformation of the acceptor chain, rather than a compact, phase segregated structure. The polydispersity of the acceptor polymer is found to play a role in the high degree of heterogeneity of energy transfer rates. In addition to providing results that could be useful for tailoring the properties of CPNs for imaging applications, these results could help provide insight into the factors affecting energy transport processes in devices containing conjugated polymer blends, such as in bulk heterojunction photovoltaic devices.

EXPERIMENTAL METHODS

Materials. The conjugated polymer poly[(9,9-dioctylfluorenyl-2,7-diyl)-*co*-(1,4-benzo-{2,1′,3}-thiadiazole)] (PFBT, MW 10 000, polydispersity 1.7) and the poly(phenylenevinylene) derivative poly[2-methoxy-5-(2-ethylhexyloxy)-1,4-phenylenevinylene] (MEH-PPV, MW 200 000, polydispersity, 4.0) were purchased from ADS Dyes, Inc. (Quebec, Canada). Fluorescein was purchased from Life Technologies. The solvent tetrahydrofuran (THF, anhydrous, inhibitor-free, 99.9%) and sodium hydroxide (NaOH, SigmaUltra, minimum 98%) were purchased from Sigma-Aldrich (Milwaukee, WI). All chemicals were used as provided without further purification.

Preparation of Nanoparticles. Conjugated polymer nanoparticles were prepared by a nanoprecipitation procedure, as described previously.[41] Stock solutions (1000 ppm) of PFBT and MEH-PPV in tetrahydrofuran (THF) were prepared by dissolving PFBT or MEH-PPV in THF with stirring. The

dx.doi.org/10.1021/jp508147r | J. Phys. Chem. C 2014, 118, 25731−25739

solutions were then diluted to 20 ppm. For blended nanoparticles, varying amounts of dopant polymer MEH-PPV solution were mixed with a solution of host polymer PFBT solution to produce mixture solutions with a total polymer concentration of 20 ppm and a ratio of MEH-PPV/PFBT ranging from 0% to 10 wt %. Then, 2 mL of each solution was rapidly injected via micropipette into 8 mL of water under sonication. The THF solvent was removed with N_2 flow at 40 °C for ∼12 h, and the nanoparticle suspension was filtered through a 0.1 μm membrane filter to remove aggregates. Typically, less than 10% of the polymer was lost during the filtration process, as determined by UV−vis absorption spectroscopy of the filtrate.

Characterization. The size distribution was determined by the atomic force microscopy (AFM). For AFM measurement, the samples were prepared by drop-casting onto glass coverslips, and the surface topography was imaged with an Ambios Q250 multimode atomic force microscope in AC mode, using a scan area of 5 μm, 500 lines/scan, and a scan rate of 0.5 Hz. UV−vis spectra were obtained using a Shimadzu UV-2101 PC scanning spectrophotometer with 1 cm quartz cuvettes. Fluorescence spectra were collected with a commercial fluorometer (Quantamaster, PTI, Inc.). All the samples used for relative fluorescence intensity measurement were diluted to yield a UV−vis absorbance of 0.1 at 473 nm.

Fluorescence lifetimes were measured in air using time-correlated single photon counting (TCSPC) spectroscopy. The method was reported in detail previously.[42] The 420 nm second harmonic of a mode-locked Ti:sapphire laser (Coherent Mira 900, 840 nm, ∼150 fs pulsewidth) was used as excitation source. Nanoparticle fluorescence was collected after passing through a 460 nm long pass filter for the unblended nanoparticles. For blended CPNs, an additional 540 ± 10 nm band pass filter was added for the blended samples to collect donor emission, while a 570 nm long pass filter was used for acceptor MEH-PPV fluorescence collection. The collected fluorescence was focused onto a single photon avalanche photodiode (iD Quantique). The resulting instrument response function (as determined from the scattering of a dilute suspension of nonfluorescent polystyrene particles) has a width of ∼80 ps (fwhm). Nonlinear least-squares fitting of the fluorescence decay kinetics to either a single exponential, biexponential, or stretched exponential (Kohlrausch−Williams−Watts, KWW) model function convolved with the instrument response function was performed using custom MATLAB scripts (Mathworks).

RESULTS AND DISCUSSION

Two well-studied conjugated polymers PFBT[43−46] and MEH-PPV[8,9,25,47] were selected as host and dopant, respectively, to prepare blended CPNs due to their excellent spectral overlap, which improves energy transfer efficiency.[38] Several blending ratios (0%, 0.5%, 1%, 2%, 4%, 6%, 10% MEH-PPV/PFBT) of PFBT/MEH-PPV nanoparticles were prepared as described above. The resulting aqueous CPN suspensions are colloidally stable and clear (shown in Figure 1a) for several months. Under 365 nm UV-lamp illumination, the CPN suspensions exhibit strong fluorescence (except 100% MEH-PPV CPNs), and gradually change color from yellow-green to orange with increasing dopant concentration, indicating efficient energy transfer from host to dopant. The diameter of CPNs is in the range of 22 ± 5 nm as determined by AFM,[38] and the blending did not appreciably affect the size distribution.

The steady-state fluorescence spectra of blended CPNs are shown in Figure 1b. As the dopant concentration increases, the fluorescence intensity of the host PFBT peak decreases, indicating effective quenching by MEH-PPV. The acceptor MEH-PPV emission increases monotonically with increasing dopant concentration up to 4% and 6% blending. At 10% dopant concentration, ∼90% of PFBT fluorescence is quenched, and the MEH-PPV emission intensity slightly decreases, likely caused by aggregation of MEH-PPV.[8,48] The MEH-PPV peaks red shift slightly from 585 to 590 nm as concentration increases, also consistent with aggregation at higher blending concentration. The quantum yield result of CPNs is shown in Table 1. The quantum yield of unblended PFBT CPNs is determined to be 0.13, while (unblended) MEH-PPV CPNs have a significantly lower quantum yield of 0.05, consistent with prior measurements.[35] When blended into PFBT nanoparticles, the overall fluorescence quantum yield increases, to up to a maximum of 0.16 (at 4% blending), confirming our hypothesis that blending with PFBT would reduce the MEH-PPV aggregation quenching and improve the brightness of CPNs.

Table 1. Total Fluorescence Quantum Yield of CPNs[a]

blending (%)	quantum yield (Φ_f)
0% (unblended)	0.13
0.5%	0.13
1%	0.14
2%	0.13
4%	0.16
6%	0.15
10%	0.13
MEH-PPV	0.05

[a]The quantum yields are obtained at λ_{ex} = 473 nm. Quantum yields were determined using fluorescein in 0.01 M NaOH as standard.

In order to obtain an initial assessment of the energy transfer processes occurring in the particles, the donor fluorescence results were fit to the Stern−Volmer equation,[49]

$$\frac{F_0}{F} = 1 + K_{sv}[f] \tag{1}$$

where F_0 and F represent the fluorescence intensities in the absence and presence of quencher, respectively, $[f]$ is the quencher/donor molecule fraction, and K_{sv} is the quenching constant. The red solid line in Figure 1c represents a linear least-squares fit to the first few points on the Stern−Volmer plot, yielding a Stern−Volmer constant of 485, indicating roughly 485 PFBT molecules are quenched by a single molecule of MEH-PPV. Because of the high energy transfer efficiency and the Poisson statistical distribution of MEH-PPV molecules in nanoparticles, there is a significant deviation from the linear Stern−Volmer relationship (blue dots represent experimental data). We introduced a nanoparticle Poisson model in a previous paper,[41] loosely based on models developed by Turro and Yekta,[50] and Tachiya[51] for quenching in micelles, in which we account for the effect of multiple quencher species per nanoparticle and a Poisson statistical distribution of quenchers. The model is given by the expression

$$\frac{F}{F_0} = \sum_n \frac{P(n, \bar{n})}{1 + nq/(1 - q)} \tag{2}$$

dx.doi.org/10.1021/jp508147r | J. Phys. Chem. C 2014, 118, 25731−25739

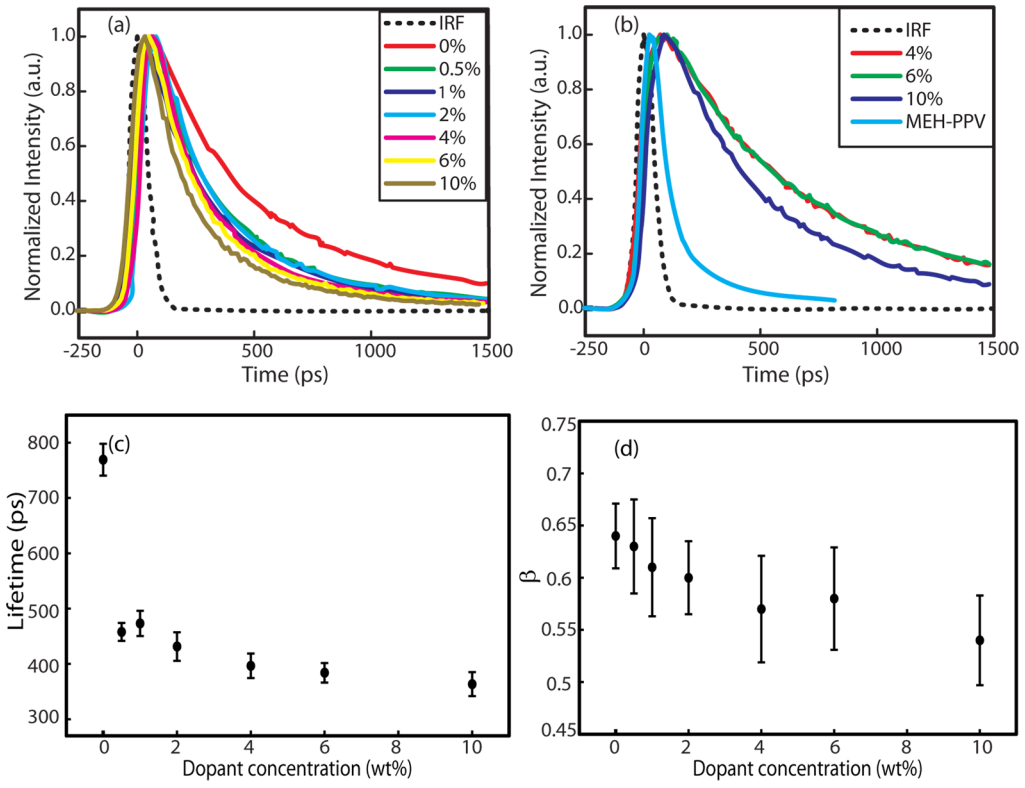

Figure 2. (a, b) Fluorescence decay traces of PFBT (a) and MEH-PPV (b) in CPNs. (c) Biexponential weighted average lifetime of donor PFBT in blended CPNs. (d) KWW fitting parameter β of donor PFBT in CPNs.

where $P(n, \bar{n})$ is the Poisson probability distribution function indicating the fraction of particles with n quenchers given an average of $\bar{n}$ quenchers per particle and q is the quenching efficiency parameter. To keep the units consistent with those used for the Stern–Volmer analysis, we calculated the average number of quenchers using the expression $\bar{n} = fN$, where f is the molecular fraction of quenchers and N is the number of donor molecules per nanoparticle. After setting the number of donor molecules to 415, based on the particle diameter, adjusting the quenching efficiency q to fit the data yields q = 0.99. The green dashed line in Figure 1c shows the fitting results. The quality of the fit is much better than that of the Stern–Volmer model, with only one adjustable parameter. Significantly, the quenching efficiency result indicates that the presence of a single MEH-PPV molecule in a nanoparticle quenches the fluorescence of the donor by 99%. This extraordinarily high quenching efficiency could be attributed to the broad absorption spectrum and large peak extinction coefficient of MEH-PPV of ~1.5×10^7 M^{-1} cm^{-1} for a polymer with a molecular weight of 200 kDa (M_w).

The high quenching efficiency provides some initial indication that the MEH-PPV likely adopts an extended conformation and is to some extent distributed throughout the nanoparticle (which would place more acceptor chromophores near the host/donor chromophores, increasing quenching efficiency), and not a highly segregated phase (which would reduce donor–acceptor interaction, reducing the quenching efficiency). Both the Stern–Volmer analysis and the Poisson model results indicate that one MEH-PPV molecule quenches hundreds of PFBT molecules. This corresponds to a quenching radius of ~12 nm, much larger than the calculated Förster radius of 9.8 nm (details of the Förster radius calculation are given in the Supporting Information). This discrepancy motivates some of the key assumptions used in modeling the energy transfer efficiency and energy transfer dynamics, discussed below.

Donor and Acceptor Excited State Kinetics. Measurements of excited state dynamics can help provide additional insight into the nature of energy transfer processes,[49] as well as providing information about the presence of aggregate states and related phenomena such as superradiance.[52,53] Decay kinetics of the fluorescent excited states for the donor PFBT and acceptor MEH-PPV in blended CPNs, as well as for the polymers in THF solution, were measured using a custom time-correlated single-photon counting (TCSPC) instrument described above. Fits to decay kinetics were obtained by nonlinear least-squares minimization, convolving a trial decay function with the instrument response function. The trial functions employed are single exponential, biexponential, and the stretched exponential (Kohlrausch–Williams–Watts, KWW) function, $F(t) = A\,e^{-(t/\tau)^{\beta}}$. The dimensionless β parameter in the KWW function represents the width of the lifetime distribution, and it ranges from 0.3, representing a broad lifetime distribution, to 1.0, representing a single lifetime.[54] Details of the fitting procedure and results are presented in the Supporting Information. The fluorescence decay of PFBT polymer dissolved in THF fits well to a single exponential decay function (τ = 3400 ps), indicating that little energy transfer to defects occurs for the dissolved polymer, since energy transfer quenching typically leads to complex decay kinetics. For unblended and blended PFBT nanoparticles (Figure 2a, c, d), the fluorescence decay of the donor PFBT is complex, as indicated by poor fit to a single exponential decay function, with systematic deviation observed in the residuals. Fits of the fluorescence decays to both biexponential and KWW

dx.doi.org/10.1021/jp508147r | J. Phys. Chem. C 2014, 118, 25731–25739

functions are good, with little systematic deviation observed in the residuals, and the weighted average lifetime (from the biexponential fit) and β of donor both decrease steadily as the MEH-PPV concentration increases, consistent with energy transfer in multichromophoric systems.[55] Fitting to a multiple energy transfer model is discussed in more detail later in this paper.

The fluorescence lifetimes of acceptor MEH-PPV in blended CPNs were measured through a 570 nm long pass filter (results shown in Table 2). The lifetime of unblended MEH-PPV nanoparticles is 130 ps. Upon blending, there is a large increase in the MEH-PPV lifetime: At MEH-PPV fractions of 4% and 6%, the average lifetime is around 1.0 ns, consistent with a significant reduction in dynamic aggregation quenching as compared to the unblended MEH-PPV case. At 10% blending, the lifetime decreases slightly (0.87 ns), consistent with the onset of aggregation quenching also apparent in the fluorescence quantum yield and slight shift in the fluorescence spectra. Interestingly, the lifetimes of MEH-PPV in the blended CPNs are higher than the lifetime of MEH-PPV in THF solution (weighted average lifetime ~440 ps). The measured fluorescence lifetime for MEH-PPV dissolved in THF is consistent with literature values.[56,57] A possible explanation for much higher lifetime in blended CPNs is that perhaps the PFBT matrix serves as a better solvent for MEH-PPV than THF, reducing aggregate formation. It is also possible that PFBT suppresses hole polaron formation in MEH-PPV, thus reducing quenching by hole polarons. The β values for MEH-PPV in blended particles are similar to that of MEH-PPV in THF (Table 2), while the β value for unblended MEH-PPV particles is 0.31, indicating a broad lifetime distribution and substantial dynamic quenching.

Table 2. MEH-PPV Weighted Average Lifetimes (τ) and β in CPNs

sample	τ (ps)	β
4%	1000	0.79
6%	980	0.74
10%	870	0.71
MEH-PPV NPs	130	0.31
MEH-PPV in THF	440	0.79

Modeling Multiple Energy Transfer in Blended CPNs. We recently developed a multiple energy transfer model and algorithm that takes into account several processes occurring in dye-doped CPNs and yields predictions for exciton decay kinetics and energy transfer efficiency. The model includes multiple energy transfer between donor chromophores (i.e., exciton diffusion), energy transfer to acceptor-dyes, confinement of excitons due to the finite particle size, and quenching by defects.[42] Here, we briefly describe the model and algorithm, as well as modifications employed to take into account the polymeric nature of the energy acceptor (MEH-PPV). Multiple energy transfer between donor chromophores (exciton diffusion) within the nanoparticle is represented by a three-dimensional random walk within a sphere. The excitons, dopants, and defects are randomly distributed within the sphere initially. At every time step, each exciton moves along each axis, with the displacement given by a Gaussian-distributed random number scaled so that $\sigma = (2D\Delta t)^{1/2}$, where D is the exciton diffusion constant and Δt is the time step (Δt = 1 ps is employed). The exciton diffusion constant is given by $D = L_D^2/2n\tau_d$, where L_D is the exciton diffusion length, n = 3 is the dimensionality of the system, and τ_d is the donor exciton lifetime. In addition to the random motion, the excitons decay (both radiatively and nonradiatively) or undergo energy transfer to an acceptor or quencher (either a quenching defect or dopant chromophore). The probability of a given exciton undergoing energy transfer to a quencher (chromophore or defect) or decay at each time step is calculated using the expression $p = 1 - e^{-k\Delta t}$, where the energy transfer rate is given by $k_{et} = \tau_d^{-1}\Sigma(R_0/R)^6$, summing over all of the acceptor or quencher species, with R_0 representing the Förster radius, R representing the distance between exciton and a given acceptor or quencher, and τ_d representing the lifetime of the donor in the absence of acceptor or quencher species. The calculated probabilities are compared to random generated numbers to determine whether the exciton undergoes energy transfer. A similar calculation is performed to determine whether the exciton undergoes radiative or nonradiative decay during the time step. If energy transfer or decay occurs, the exciton is removed from the population. Iteration continues over all excitons until nearly all the excitons have decayed or quenched. The simulations are carried out for many different sets of random initial configurations of acceptors and excitons, and the quenching efficiency and exciton dynamics are calculated from the averaged results.

Next we discuss intrinsic defects and how they are included in the model. For the unblended PFBT nanoparticles, the quantum yield, excited state lifetime, and KWW parameter β are significantly reduced (ϕ_{un} = 0.13, τ_{avg} = 770 ps, β = 0.64) as compared to the case of the PFBT polymer in THF (ϕ_p = 0.66, τ_{avg} = 3400 ps, β = 1). The decrease of these parameters is likely caused by the presence of quenching species inside the particle, which we refer to here as defects. The defects could include oxidized species, aggregates, photogenerated hole polarons, excimers, exciplexes, or other quenching species.[58−61] We previously showed that photogenerated hole polarons act as highly efficient quenchers in CPNs.[30] The reduced fluorescence quantum yield and average lifetime and the increase of lifetime heterogeneity (β value decrease) for the CPNs are prima facie evidence of the existence of a dynamic quenching species or process, and that quenching is to some degree suppressed by dissolving the polymer in a good solvent, indicating that energy transfer could be involved, since energy transfer rates (for both donor−donor and donor−acceptor transfer) are highly dependent on interchromophore distance, and the chromophore spacing is sensitive to solvent conditions. In the case of polarons acting as quenchers, another possible explanation for the increased quenching in CPNs dispersed in water as compared to the polymer dissolved in an organic solvent could be that the aqueous environment likely favors polaron formation, due to the high dielectric constant as compared to organic solvents. Based on the observation that quenching by defects is significantly reduced for the polymer dissolved in good solvent as compared to the nanoparticle or film, the quenching efficiency of the defects (η_d) is calculated as 0.80 from the fluorescence quantum yields of PFBT polymer in THF and PFBT CPNs by the expression $\eta_d = 1 - \phi_{un}/\phi_p$.

We included defect quenching by representing defects as nonfluorescent energy acceptors with a Förster radius of 4 nm, adjusting the level of defects until the kinetics and fluorescence quantum yield were in approximate agreement with experimental results for unblended PFBT CPNs, using the approach discussed previously.[42] Since the number of defects per CPN is

dx.doi.org/10.1021/jp508147r | J. Phys. Chem. C 2014, 118, 25731−25739

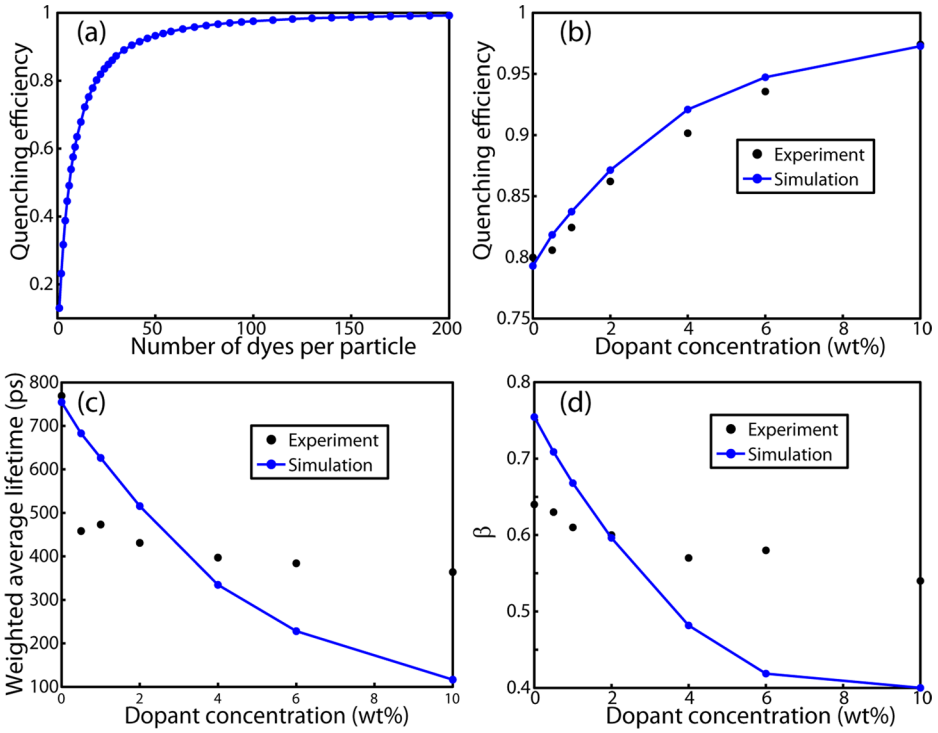

Figure 3. (a) Quenching efficiency of initial exciton diffusion simulations. (b–d) Comparison of simulated (blue dot with line) and experimental (black dot) data: (b) quenching efficiency, (c) average lifetime, and (d) KWW stretch parameter β, vs dopant concentration (wt %).

likely to follow a Poisson distribution, the defect density was estimated by comparison of model calculations to the CPN fluorescence quantum yield and fluorescence decay kinetics as follows. First, the initial exciton diffusion simulation is performed by varying the dye (quencher) number per particle with lifetime of PFBT in THF (3400 ps), particle radius r = 11 nm (from AFM result), exciton diffusion length L_D = 12 nm, and Förster radius R_0 = 4 nm. The quenching efficiency and exciton decay kinetics for various numbers of dyes per particle are obtained from exciton diffusion simulations described above. The simulated quenching efficiency versus number of dyes per particle is shown in Figure 3a. Second, the population of nanoparticles is described by an average defect density parameter (average number of defects per particle), with the fraction of particles containing a given number of defects given by the Poisson distribution. From the distribution weights and the simulation results, a weighted average quenching efficiency is obtained, and similarly, population-averaged decay kinetics traces are obtained and fit to a biexponential and KWW functions to obtain the average lifetime and β parameter. The average defect density is varied until a good agreement with experimental data is obtained, yielding an average defect density of 20 dye equivalents per 22 nm diameter particle. At this average defect density, the simulated result for the PFBT particle is η_d = 0.79, τ_{avg} = 750 ps, and β = 0.75. The quenching efficiency and averaged lifetime are consistent with the experimental data (η_d = 0.80, τ_{avg} = 770 ps). The slightly lower experimental KWW stretch parameter β (0.64) for the experimental data as compared to the simulated result (0.75) perhaps indicates an additional process or effect leading to broadening of the lifetime distribution.

The quenching efficiency values of the blended CPNs given in Figure 3b are given by the equation $\eta = \eta_d + (1 - \eta_d)(1 - F/F_0)$, where F_0 and F represent the nanoparticle fluorescence intensities of unblended and blended CPNs, respectively. The calculation of quenching efficiency of the polymer is obtained from the exciton diffusion and energy transfer results (Figure 3a) as follows. As stated above, the high quenching efficiency of MEH-PPV indicates that the molecule likely exhibits an open or extended conformation. Since the conformation or conformational distribution is not known and for the sake of computational simplicity, we represent the extended MEH-PPV chain as isolated chromophores randomly distributed throughout the particle. This is a gross simplification that is likely to overestimate quenching efficiency, since a more realistic beads-on-a-string picture would result in correlation between chromophore positions (i.e., there will typically be 1–2 chromophores within ~1 nm of a given chromophore), resulting in overlap of quenching volumes, likely resulting in a reduced quenching efficiency. On the other hand, assuming a random distribution of chromophores places some in closer proximity than would a space-filling bead model, so there could be some cancellation of errors.

A likely more significant issue is the polydispersity of the acceptor polymer. If we ignore the polydispersity of acceptor and assume molecular weight 206 000 with PDI = 1 in the model, the resulting quenching efficiencies are lower than the experimental data for most blending ratios (shown in Supporting Information, Figure S1) since there are some particles which do not contain acceptor based on Poisson statistics. Here we discuss how acceptor polydispersity is included in the model. Gel permeation chromatography (GPC) yields M_n = 47 400, M_w = 206 000, and a polydispersity index (PDI) of 4.3. For modeling purposes, we represent the polymer weight distribution as a mixture of four different polymer components with molecular weights of 3900, 10 400, 104 000, and 312 000, and number (molecule) fractions for each component of 0.47, 0.26, 0.17, and 0.1. The molecular weight

dx.doi.org/10.1021/jp508147r | J. Phys. Chem. C 2014, 118, 25731–25739

distribution of the mixture is M_n = 53 400, M_w = 217 000, and PDI = 4.1, close to the GPC results. The distribution of the various molecular weight polymer chains in the particles is calculated using the Poisson distribution (i.e., it is assumed that the dopant polymer chains are randomly distributed among particles) based on the weight fraction of MEH-PPV (per nanoparticle) and the population fractions for each molecular weight, using the expression $N_i = M_{NP} f_d f_i / M_i$, where N_i is the number of chains of a given component i, M_{NP} is the mass of nanoparticle, f_d is the blending fraction, f_i is the molecule fraction of component i, and M_i is the mass of component i. For a given nanoparticle containing a number of polymer chains of various molecular weights, the number of MEH-PPV chromophores is calculated based on the following reasoning. An MEH-PPV chromophore is composed of 4−8 repeat units.[62−64] If we assume that 5 repeat units is one chromophore (∼1300 Da), then a straightforward calculation (based on the peak extinction coefficient MEH-PPV polymer mentioned earlier) yields a peak extinction coefficient per chromophore of $\sim 4 \times 10^5$ M^{-1} cm^{-1}. We treat the chromophore size as an adjustable simulation parameter, and used a value of 5 monomer units per chromophore in the simulations. For the sake of reducing calculation complexity, we assume that each chromophore is roughly equivalent to one perylene red molecule, which in terms of the simulation means that each chromophore is represented as a point acceptor with a Förster radius of 4 nm, which is the same as the Förster radius used to represent the defects. Thus, the total number of energy acceptors in a nanoparticle is given as the sum of the number of defects and the number of MEH-PPV chromophores.

A statistical sample of CPNs, representing the distribution of defects and polymer chains, is generated, and for each CPN the total number of acceptors is calculated using the method described above. From the distribution, the population average quenching efficiencies and kinetics are calculated. The simulated population-averaged kinetics trace is fit to biexponential and KWW functions to obtain weighted average lifetimes and KWW stretch parameter β, for each blending ratio, which are given in Figure 3b−d. The agreement between the simulated quenching efficiency and the experimental results is good, while the lifetime and β simulated results agree reasonably well with the experimental results for much of the range of blending levels, with systematic deviations at the lower and higher blending levels. While the cause of the deviation cannot be determined conclusively, the somewhat poor agreement is not surprising given the number of simplifications and assumptions in the model. Even for the simpler case of dye-doped PFBT CPNs, the fit of lifetime and β was not particularly good.[42] Possible causes or explanations are discussed below.

First, for the case of higher blending concentration, the short lifetime and small β represent an experimental difficulty since there are likely some significant short lifetime components in the decay trace that are not resolved with the TCSPC apparatus. For example, at 10% MEH-PPV blending, there is a significant ∼3 ps lifetime component when fitting the first few points of simulated population kinetics to a single exponential decay function. This short-lived component is well below the ∼80 ps experimental resolution. Short-lived components also contribute few photons to the kinetics trace, which can make them difficult to measure. Also complicating the determination of short-lived components is the fact that a small amount of scattered laser light or autofluorescence can overlap with the kinetic trace at early times.

Additional effects and processes that we have not included in the model could also affect the overall energy transfer rate and the width of the distribution of rates, such as heterogeneous or dispersive exciton transport caused by energetic heterogeneity[65] and particle-to-particle variations arising from the particle size distribution. Additionally, the acceptor chain conformation is not included in the current model. Furthermore, the current model is essentially a continuum model, and it is likely that a more granular model that explicitly includes individual donor and acceptor chromophores would yield a smaller distribution of donor−acceptor distances and thus a smaller distribution of energy transfer rates, which could improve agreement between the model and experiment. It is also possible that adjacent PFBT and MEH-PPV chromophores could result in mostly static quenching of the PFBT chromophore, which could explain the fact that the measured lifetimes appear to be less sensitive to blending concentration than predicted by the model, which assumes mostly dynamic quenching. Further development of the model for blended conjugated polymer nanoparticle is planned, including treating the polymer chain as dye/beads-on-a-string, and replacing the continuum approach with one that includes discrete donor and acceptor chromophores. Additional experiments using dopant polymers with a lower polydispersity index are planned and could also serve as a useful test of model assumptions and the effect of polydispersity on the distribution of energy transfer rates.

CONCLUSION

In summary, blended PFBT/MEH-PPV CPNs exhibit efficient energy transfer as indicated by the efficient quenching of the donor (PFBT) polymer fluorescence and strong acceptor (MEH-PPV) fluorescence at low to moderate fractions of MEH-PPV. Stern−Volmer analysis and nanoparticle quenching analysis of the steady-state quenching efficiency results indicate that a single MEH-PPV chain within a 22 nm diameter particle quenches ∼99% of the donor fluorescence, consistent with a quenching radius of several tens of nanometers. Somewhat surprisingly, the blended CPNs exhibit a higher fluorescence quantum yield as compared to particles containing only PFBT. This phenomenon of increased brightness for blended CPNs could be useful for improving sensitivity in imaging and sensing, and points to a possible strategy for improving electro-optic device efficiency. Additional insight into the nature of energy transfer processes in blended conjugated polymers was obtained from picosecond fluorescence lifetime measurements and comparison to a multiple energy transfer model. Donor exciton lifetime reduction and lifetime distribution broadening with increase of blending were determined by picosecond fluorescence lifetime measurement, indicating a broad range of energy transfer rates. Agreement between experiment and model results for quenching efficiency is very good, and the differences between the simulated lifetime and β value and the time-resolved experimental data can be explained by some of the assumptions of the model (including the assumption that dynamic quenching predominates) and the limitations of the measurement. Our results indicate that both exciton diffusion and polydispersity of acceptor are the major factors in determining the quenching efficiency and energy transfer rates in blended conjugated polymer systems. These results help provide the basis for additional studies aimed at understanding the unusual fluorescence properties of PFBT/MEH-PPV nanoparticles including anomalous saturation behavior and photoswitching. Additionally, the results shed

dx.doi.org/10.1021/jp508147r | J. Phys. Chem. C 2014, 118, 25731−25739

light on the complex exciton diffusion and energy transfer processes occurring in devices that include blended polymers, such as bulk heterojunction photovoltaic devices. Furthermore, the results indicate that quenching by defects (likely polarons) could limit performance of electro-optic devices, and that blending can, in some cases, improve performance, by providing a competitive energy transfer pathway. The results also clearly show that the conformation (e.g., extended/solvated versus collapsed chains forming nanoparticles) has a profound effect on key optical properties such as fluorescence quantum yield, likely due to increased energy transfer and exciton diffusion in the collapsed, nanoparticle conformation. The effect of the host polymer on polaron stability is also a likely factor. Finally, the results indicate the importance of measuring rates in complex systems using time-resolved methods, rather than adducing rates from steady-state measurements. For a simple system characterized by a single (dynamic) quenching rate constant k_q, the quenching efficiency is given by a simple expression such as $Q = k_q/k_{tot}$, which can be rearranged to yield the rate constant, whereas for a complex system involving multiple rates and possibly static quenching the relationship is complex, requiring a more direct measure of the rates involved. Indeed, while the (steady-state) quenching efficiencies are reproduced quite well by the model, the distribution of energy transfer rates obtained from the model are not in agreement with the time-resolved results, clearly indicating of the importance of time-resolved measurements in this case.

■ ASSOCIATED CONTENT

Supporting Information

Details of fluorescence quantum yield determination, Förster radius calculation, picosecond fluorescence lifetime fitting results, and radiative and nonradiative rates. This material is available free of charge via the Internet at http://pubs.acs.org.

■ AUTHOR INFORMATION

Corresponding Author

*E-mail: mcneill@clemson.edu.

Notes

The authors declare no competing financial interest.

■ ACKNOWLEDGMENTS

We acknowledge financial support from the NSF under Grant No. CHE-1058885.

■ REFERENCES

(1) McQuade, D. T.; Pullen, A. E.; Swager, T. M. Conjugated Polymer-Based Chemical Sensors. *Chem. Rev.* **2000**, *100*, 2537−2574.
(2) Thomas, S. W.; Joly, G. D.; Swager, T. M. Chemical Sensors Based on Amplifying Fluorescent Conjugated Polymers. *Chem. Rev.* **2007**, *107*, 1339−1386.
(3) Gunes, S.; Neugebauer, H.; Sariciftci, N. S. Conjugated Polymer-Based Organic Solar Cells. *Chem. Rev.* **2007**, *107*, 1324−1338.
(4) Gustafsson, G.; Cao, Y.; Treacy, G. M.; Klavetter, F.; Colaneri, N.; Heeger, A. J. Flexible Light-Emitting-Diodes Made from Soluble Conducting Polymers. *Nature* **1992**, *357*, 477−479.
(5) Sirringhaus, H.; Tessler, N.; Friend, R. H. Integrated Optoelectronic Devices Based on Conjugated Polymers. *Science* **1998**, *280*, 1741−1744.
(6) Scherf, U.; List, E. J. W. Semiconducting Polyfluorenes-Towards Reliable Structure-Property Relationships. *Adv. Mater.* **2002**, *14*, 477−487.
(7) Chen, T. A.; Wu, X. M.; Rieke, R. D. Regiocontrolled Synthesis of Poly(3-Alkylthiophenes) Mediated by Rieke Zinc-Their Characterization and Solid-State Properties. *J. Am. Chem. Soc.* **1995**, *117*, 233−244.
(8) Schwartz, B. J. Conjugated Polymers as Molecular Materials: How Chain Conformation and Film Morphology Influence Energy Transfer and Interchain Interactions. *Annu. Rev. Phys. Chem.* **2003**, *54*, 141−172.
(9) Huser, T.; Yan, M.; Rothberg, L. J. Single Chain Spectroscopy of Conformational Dependence of Conjugated Polymer Photophysics. *Proc. Natl. Acad. Sci. U. S. A.* **2000**, *97*, 11187−11191.
(10) Yu, G.; Heeger, A. J. Charge Separation and Photovoltaic Conversion in Polymer Composites with Internal Donor-Acceptor Heterojunctions. *J. Appl. Phys.* **1995**, *78*, 4510−4515.
(11) Chen, J. W.; Cao, Y. Development of Novel Conjugated Donor Polymers for High-Efficiency Bulk-Heterojunction Photovoltaic Devices. *Acc. Chem. Res.* **2009**, *42*, 1709−1718.
(12) Berggren, M.; Inganas, O.; Gustafsson, G.; Rasmusson, J.; Andersson, M. R.; Hjertberg, T.; Wennerstrom, O. Light-Emitting-Diodes with Variable Colors from Polymer Blends. *Nature* **1994**, *372*, 444−446.
(13) Halls, J. J. M.; Walsh, C. A.; Greenham, N. C.; Marseglia, E. A.; Friend, R. H.; Moratti, S. C.; Holmes, A. B. Efficient Photodiodes from Interpenetrating Polymer Networks. *Nature* **1995**, *376*, 498−500.
(14) Alam, M. M.; Jenekhe, S. A. Efficient Solar Cells from Layered Nanostructures of Donor and Acceptor Conjugated Polymers. *Chem. Mater.* **2004**, *16*, 4647−4656.
(15) Kasha, M.; Rawls, H. R.; El-Bayoumi, M. A. The Exciton Model in Molecular Spectroscopy. *Pure Appl. Chem.* **1965**, *11*, 371−392.
(16) Bardeen, C. J. The Structure and Dynamics of Molecular Excitons. *Annu. Rev. Phys. Chem.* **2014**, *65*, 127−148.
(17) Förster, T. Intermolecular Energy Migration and Fluorescence. *Ann. Phys.* **1948**, *2*, 55−75.
(18) Burlakov, V. M.; Kawata, K.; Assender, H. E.; Briggs, G. A. D.; Ruseckas, A.; Samuel, I. D. W. Discrete Hopping Model of Exciton Transport in Disordered Media. *Phys. Rev. B* **2005**, *72*, 075206−1−075206−5.
(19) Scholes, G. D.; Rumbles, G. Excitons in Nanoscale Systems. *Nat. Mater.* **2006**, *5*, 683−696.
(20) Haugeneder, A.; Neges, M.; Kallinger, C.; Spirkl, W.; Lemmer, U.; Feldmann, J.; Scherf, U.; Harth, E.; Gugel, A.; Mullen, K. Exciton Diffusion and Dissociation in Conjugated Polymer Fullerene Blends and Heterostructures. *Phys. Rev. B* **1999**, *59*, 15346−15351.
(21) List, E. J. W.; Creely, C.; Leising, G.; Schulte, N.; Schluter, A. D.; Scherf, U.; Mullen, K.; Graupner, W. Excitation Energy Migration in Highly Emissive Semiconducting Polymers. *Chem. Phys. Lett.* **2000**, *325*, 132−138.
(22) Shaw, P. E.; Ruseckas, A.; Samuel, I. D. W. Exciton Diffusion Measurements in Poly(3-hexylthiophene). *Adv. Mater.* **2008**, *20*, 3516−3520.
(23) Hennebicq, E.; Pourtois, G.; Scholes, G. D.; Herz, L. M.; Russell, D. M.; Silva, C.; Setayesh, S.; Grimsdale, A. C.; Mullen, K.; Bredas, J. L.; Beljonne, D. Exciton Migration in Rigid-Rod Conjugated Polymers: An Improved Forster Model. *J. Am. Chem. Soc.* **2005**, *127*, 4744−4762.
(24) Dias, F. B.; Knaapila, M.; Monkman, A. P.; Burrows, H. D. Fast and Slow Time Regimes of Fluorescence Quenching in Conjugated Polyfluorene-Fluorenone Random Copolymers: The Role of Exciton Hopping and Dexter Transfer along the Polymer Backbone. *Macromolecules* **2006**, *39*, 1598−1606.
(25) Yu, J.; Hu, D. H.; Barbara, P. F. Unmasking Electronic Energy Transfer of Conjugated Polymers by Suppression of O(2) Quenching. *Science* **2000**, *289*, 1327−1330.
(26) Hooley, E. N.; Tilley, A. J.; White, J. M.; Ghiggino, K. P.; Bell, T. D. M. Energy Transfer in PPV-Based Conjugated Polymers: A Defocused Widefield Fluorescence Microscopy Study. *Phys. Chem. Chem. Phys.* **2014**, *16*, 7108−7114.
(27) Hu, D. H.; Yu, J.; Padmanaban, G.; Ramakrishnan, S.; Barbara, P. F. Spatial Confinement of Exciton Transfer and the Role of

Conformational Order in Organic Nanoparticles. *Nano Lett.* **2002**, *2*, 1121−1124.
(28) Tenery, D.; Worden, J. G.; Hu, Z. J.; Gesquiere, A. J. Single Particle Spectroscopy on Composite MEH-PPV/PCBM Nanoparticles. *J. Lumin.* **2009**, *129*, 423−429.
(29) Hu, Z. J.; Tenery, D.; Bonner, M. S.; Gesquiere, A. J. Correlation between Spectroscopic and Morphological Properties of Composite P3HT/PCBM Nanoparticles Studied by Single Particle Spectroscopy. *J. Lumin.* **2010**, *130*, 771−780.
(30) Yu, J. B.; Wu, C. F.; Tian, Z. Y.; McNeill, J. Tracking of Single Charge Carriers in a Conjugated Polymer Nanoparticle. *Nano Lett.* **2012**, *12*, 1300−1306.
(31) Yu, J. B.; Wu, C. F.; Sahu, S. P.; Fernando, L. P.; Szymanski, C.; McNeill, J. Nanoscale 3D Tracking with Conjugated Polymer Nanoparticles. *J. Am. Chem. Soc.* **2009**, *131*, 18410−18414.
(32) Wu, C. F.; Bull, B.; Christensen, K.; McNeill, J. Ratiometric Single-Nanoparticle Oxygen Sensors for Biological Imaging. *Angew. Chem., Int. Ed.* **2009**, *48*, 2741−2745.
(33) Chan, Y. H.; Wu, C. F.; Ye, F. M.; Jin, Y. H.; Smith, P. B.; Chiu, D. T. Development of Ultrabright Semiconducting Polymer Dots for Ratiometric pH Sensing. *Anal. Chem.* **2011**, *83*, 1448−1455.
(34) Childress, E. S.; Roberts, C. A.; Sherwood, D. Y.; LeGuyader, C. L. M.; Harbron, E. J. Ratiometric Fluorescence Detection of Mercury Ions in Water by Conjugated Polymer Nanoparticles. *Anal. Chem.* **2012**, *84*, 1235−1239.
(35) Wu, C.; Bull, B.; Szymanski, C.; Christensen, K.; McNeill, J. Multicolor Conjugated Polymer Dots for Biological Fluorescence Imaging. *ACS Nano* **2008**, *2*, 2415−2423.
(36) Wu, C. F.; Schneider, T.; Zeigler, M.; Yu, J. B.; Schiro, P. G.; Burnham, D. R.; McNeill, J. D.; Chiu, D. T. Bioconjugation of Ultrabright Semiconducting Polymer Dots for Specific Cellular Targeting. *J. Am. Chem. Soc.* **2010**, *132*, 15410−15417.
(37) Wu, C. F.; Chiu, D. T. Highly Fluorescent Semiconducting Polymer Dots for Biology and Medicine. *Angew. Chem., Int. Ed.* **2013**, *52*, 3086−3109.
(38) Wang, X. L.; Groff, L. C.; McNeill, J. D. Photoactivation and Saturated Emission in Blended Conjugated Polymer Nanoparticles. *Langmuir* **2013**, *29*, 13925−13931.
(39) Bretschneider, S.; Eggeling, C.; Hell, S. W. Breaking the Diffraction Barrier in Fluorescence Microscopy by Optical Shelving. *Phys. Rev. Lett.* **2007**, *98*, 218103−1−218103−4.
(40) Patterson, G.; Davidson, M.; Manley, S.; Lippincott-Schwartz, J. Superresolution Imaging using Single-Molecule Localization. *Annu. Rev. Phys. Chem.* **2010**, *61*, 345−367.
(41) Wu, C. F.; Peng, H. S.; Jiang, Y. F.; McNeill, J. Energy Transfer Mediated Fluorescence from Blended Conjugated Polymer Nanoparticles. *J. Phys. Chem. B* **2006**, *110*, 14148−14154.
(42) Groff, L. C.; Wang, X. L.; McNeill, J. D. Measurement of Exciton Transport in Conjugated Polymer Nanoparticles. *J. Phys. Chem. C* **2013**, *117*, 25748−25755.
(43) Wu, W. C.; Liu, C. L.; Chen, W. C. Synthesis and Characterization of New Fluorene-Acceptor Alternating and Random Copolymers for Light-Emitting Applications. *Polymer* **2006**, *47*, 527−538.
(44) Zaumseil, J.; Donley, C. L.; Kim, J. S.; Friend, R. H.; Sirringhaus, H. Efficient Top-Gate, Ambipolar, Light-Emitting Field-Effect Transistors Based on a Green-Light-Emitting Polyfluorene. *Adv. Mater.* **2006**, *18*, 2708−2712.
(45) Stevens, M. A.; Silva, C.; Russell, D. M.; Friend, R. H. Exciton Dissociation Mechanisms in the Polymeric Semiconductors Poly(9,9-dioctylfluorene) and Poly(9,9-dioctylfluorene-co-benzothiadiazole). *Phys. Rev. B* **2001**, *63*, 165213−1−165213−18.
(46) Donley, C. L.; Zaumseil, J.; Andreasen, J. W.; Nielsen, M. M.; Sirringhaus, H.; Friend, R. H.; Kim, J. S. Effects of Packing Structure on the Optoelectronic and Charge Transport Properties in Poly(9,9-di-n-octylfluorene-alt-benzothiadiazole). *J. Am. Chem. Soc.* **2005**, *127*, 12890−12899.
(47) Nguyen, T. Q.; Martini, I. B.; Liu, J.; Schwartz, B. J. Controlling Interchain Interactions in Conjugated Polymers: The Effects of Chain Morphology on Exciton-Exciton Annihilation and Aggregation in MEH-PPV Films. *J. Phys. Chem. B* **2000**, *104*, 237−255.
(48) Nguyen, T. Q.; Doan, V.; Schwartz, B. J. Conjugated Polymer Aggregates in Solution: Control of Interchain Interactions. *J. Chem. Phys.* **1999**, *110*, 4068−4078.
(49) Lakowicz, J. R. *Principles of Fluorescence Spectroscopy*, third ed.; Springer: New York, 2006.
(50) Turro, N. J.; Yekta, A. Luminescent Probes for Detergent Solutions - Simple Procedure for Determination of Mean Aggregation Number of Micelles. *J. Am. Chem. Soc.* **1978**, *100*, 5951−5952.
(51) Tachiya, M. Application of a Generating Function to Reaction-Kinetics in Micelles-Kinetics of Quenching of Luminescent Probes in Micelles. *Chem. Phys. Lett.* **1975**, *33*, 289−292.
(52) Deboer, S.; Wiersma, D. A. Dephasing-Induced Damping of Superradiant Emission in J-Aggregates. *Chem. Phys. Lett.* **1990**, *165*, 45−53.
(53) Meinardi, F.; Cerminara, M.; Sassella, A.; Bonifacio, R.; Tubino, R. Superradiance in Molecular H Aggregates. *Phys. Rev. Lett.* **2003**, *91*, 247401−1−247401−4.
(54) Chen, R. Apparent Stretched-Exponential Luminescence Decay in Crystalline Solids. *J. Lumin.* **2003**, *102*, 510−518.
(55) Gammill, L. S.; Powell, R. C. Energy-Transfer in Perylene Doped Anthracene-Crystals. *Mol. Cryst. Liq. Cryst.* **1974**, *25*, 123−130.
(56) Smilowitz, L.; Hays, A.; Heeger, A. J.; Wang, G.; Bowers, J. E. Time-Resolved Photoluminescence from Poly[2-methoxy, 5-(2′-ethylhexyloxy)-p-phenylene-vinylene]-Solutions, Gels, Films, and Blends. *J. Chem. Phys.* **1993**, *98*, 6504−6509.
(57) Samuel, I. D. W.; Rumbles, G.; Collison, C. J.; Friend, R. H.; Moratti, S. C.; Holmes, A. B. Picosecond Time-Resolved Photoluminescence of PPV Derivatives. *Synth. Met.* **1997**, *84*, 497−500.
(58) Yan, M.; Rothberg, L. J.; Papadimitrakopoulos, F.; Galvin, M. E.; Miller, T. M. Defect Quenching of Conjugated Polymer Luminescence. *Phys. Rev. Lett.* **1994**, *73*, 744−747.
(59) Bolinger, J. C.; Traub, M. C.; Adachi, T.; Barbara, P. F. Ultralong-Range Polaron-Induced Quenching of Excitons in Isolated Conjugated Polymers. *Science* **2011**, *331*, 565−567.
(60) Jenekhe, S. A.; Osaheni, J. A. Excimers and Exciplexes of Conjugated Polymers. *Science* **1994**, *265*, 765−768.
(61) Jakubiak, R.; Collison, C. J.; Wan, W. C.; Rothberg, L. J.; Hsieh, B. R. Aggregation Quenching of Luminescence in Electroluminescent Conjugated Polymers. *J. Phys. Chem. A* **1999**, *103*, 2394−2398.
(62) Holzer, W.; Penzkofer, A.; Tillmann, H.; Horhold, H. H. Spectroscopic and Travelling-Wave Lasing Characterisation of Gilch-Type and Horner-Type MEH-PPV. *Synth. Met.* **2004**, *140*, 155−170.
(63) De Leener, C.; Hennebicq, E.; Sancho-Garcia, J. C.; Beljonne, D. Modeling the Dynamics of Chromophores in Conjugated Polymers: The Case of Poly (2-methoxy-5-(2′-ethylhexyl)oxy 1,4-phenylene vinylene) (MEH-PPV). *J. Phys. Chem. B* **2009**, *113*, 1311−1322.
(64) Kohler, A.; Hoffmann, S. T.; Bassler, H. An Order-Disorder Transition in the Conjugated Polymer MEH-PPV. *J. Am. Chem. Soc.* **2012**, *134*, 11594−11601.
(65) Barbara, P. F.; Gesquiere, A. J.; Park, S. J.; Lee, Y. J. Single-Molecule Spectroscopy of Conjugated Polymers. *Acc. Chem. Res.* **2005**, *38*, 602−610.